university of groningen / faculty of mathematics and natural sciences

Chemoenzymatic dimerization of single domain antibodies for multimodal imaging.

Master report II
Jerre Edens
s1875140
Supervisor 1: M. Rashidian
Supervisor 2: M. H. K. Linskens
Ploegh lab
Whitehead Institute for Biomedical Research

Whitehead Institute

Abstract

Camelid derived single domain antibody fragments (VHH) are small sized, have rapid circulatory clearance and great binding specificity. Because immune cells can infiltrate tumors, VHHs specifically binding MHC Class II or CD11b can therefore be utilized for cancer detection and the presence of malignancy. VHHs consist of only a single domain, so their binding affinity may entail constrains compared to the natural bivalent antibodies. During this project a chemoenzymatic dimerization approach was developed to enhance the resemblance of these fragments to natural antibodies. Since the specific binding site of the VHH is positioned away from its C-terminus, C-terminal motif LPETG is utilized for sortagging with a linker, enabling dimerization via biorthogonal click chemistry. This linker also allowed the appending of a fluorophore or ^{18}F, which was used for biological evaluation. The dimers were analyzed with *in vitro* FACS studies and *in vivo* two-photon microscopy to obtain an assessment of their binding affinity and compare them with their corresponding monomer. Eventually *in vivo* PET imaging clearly showed lymphoid organs and engrafted tumors infiltrated by immune cells with significant improvement in signal strength.

Contents

Introduction

Cancer immunotherapy

Immunotherapy is a treatment which uses the immune system to fight diseases like cancer. It has become an auspicious treatment and therefore numerous research groups perform studies to improve this therapy[1]. For cancer immunotherapy, the natural body's defense is stimulated to work harder or smarter to attack tumors. This is supported by the extensive infiltration of immune cells in tumors[2,3]. The cancer treatment can be achieved by stopping or slowing down the tumor growth, stopping cancer from spreading to other parts of the body or improving the immune system by stimulating the immune system to obliterate tumors. Although the way in which immunotherapy operates is not always completely understood, there are now multiple ways of applying this therapy. Recently cancer vaccines have been developed to prevent cervical cancer[4]. Where vaccines are known for immunization of humans against other diseases, this technique is nowadays also applicable for certain cancers in a preventive fashion. Another way of therapy is the use of immune checkpoint inhibitors[5]. These checkpoints are defined by immunologist as highly effective targets for antibody-based interventions. One of the most advanced techniques utilizing these checkpoints is the use of monoclonal antibodies (mAbs).

Antibodies are expressed to detect antigens or specific proteins in the body. They are part of the natural defense mechanism against foreign and harmful substances[6]. mAbs are designed in a laboratory and produced by immune cells which are all similar[1]. These immune cells are all clones from a parent cell and that is where the name monoclonal is derived from. All the mAbs are exactly the same and thus bind to the same sequence of amino acids (epitope). Therefore a mAb can be designed in laboratories to only bind to a specific protein in cells and not harm any other protein. In cancer immunotherapy, mAbs can be applied in multiple ways:

- mAbs were designed for binding essential membrane proteins of cancer cells or immune cells. One of the main immunosuppressing characteristics of tumors is the protein PD-L1 expressed on the cancer cell membrane. It binds PD-1 on immune cells causing a cascade of protein interactions resulting in the inactivation of the immune system. By blocking PD-1 or PD-L1, this interaction will not take place allowing the immune cell to attack cancer cells (Figure 1)[7,8].

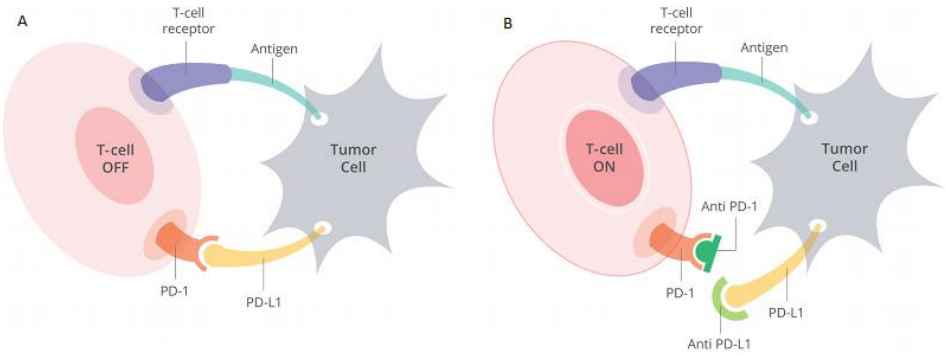

Figure 1. A) Deactivation of T-cells by PD-1/PD-L1 recognition and B) activation of the T-cell by blocking PD-L1 and PD1.

- mAbs against PD-L1 can specifically bind cancer cells, but there are more receptors (checkpoints) which can be used for therapies. CD30 is a cell membrane protein of the tumor necrosis factor receptor family and tumor marker. mAbs which bind to CD30 were developed and enabled direct delivery of the drugs to the tumor marker and thereby attacking the cancer cells specifically[9].

- The growth of blood vessel in tumors is dependent on multiple growth factors. mAbs against Vascular endothelial growth factor (VEGF) have shown to suppress angiogenesis in a variety of human tumor cells[10]. Inhibiting neovascularization in tumors often suppresses tumor growth.

- Besides direct obliterating cancer cells, mAbs can also be used for imaging and diagnosing tumors. mAbs functionalized with for instance a radioactive compound accumulate in tumors and can be visualized with positron emission tomography (PET) imaging. Mesothelin (MSLN) cell differentiation-associated glycoprotein expressed in pancreatic or ovarian cancer was targeted by a monoclonal antibody conjugated to ^{64}Cu. Subsequent *in vitro* and *in vivo* PET imaging showed that this was a suitable tumor imaging method[11].

Another successful way of imaging tumors is by the use of ^{18}F-2-fluoro-2-deoxy-D-glucose positron emission tomography (FDG-PET)[12]. Because tumors have high metabolic activity, they have a higher uptake of glucose compared to other tissue. This results in a higher radioactivity in tumors and can be detected with a PET scan. However this detection method does not provide information on immune cells in the tumor micro environment. The specific binding characteristics of the mAbs make them suitable for not only detailed tumor detection by binding tumors but also elaborate on the immune cells in the tumor micro environment. Tools to track MHC Class II, CD11b or CD8 on immune cells have been developed and have proven to be a promising method for detecting immune cells in the tumor micro environment[13-15].

VHHs

mAbs are large in size (150 kDa) and can sustain in the bloodstream for several days[16] (Figure 2A). Their size also prevents them from penetrating into tissue efficiently[17,18]. Therefore shrunk antibodies have been produced in the lab, but these proteins are still in the ~40-50 kDa range (diabodies)[19] or 20 kDa single-chain variable fragments (scFv fragments)[20]. Diabodies are fused variable fragments of two different antibodies (Figure 2B). scFv fragments entail only the variable parts of the heavy and light chain of an antibody (Figure 2C).

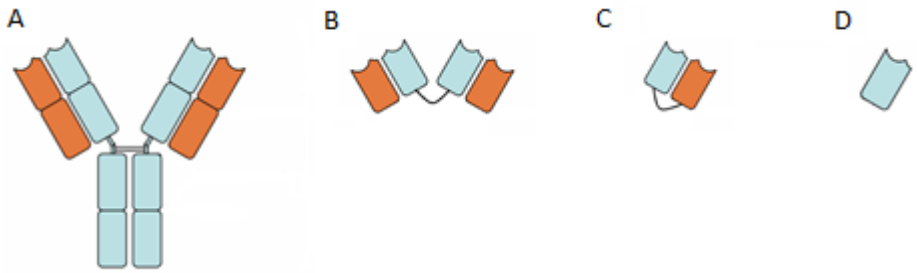

Figure 2. A. Full size antibody. B. Diabodies: two heavy and light chain fragments genetically fused. C. scFv fragments: one heavy and one light chain genetically fused. D. VHH: single domain antibody.

The labeling and purification of these fragments has shown to be difficult. Recently camelid antibodies entailing only heavy domains have been discovered. Because of the absence of the light domain, these antibodies have a single monomeric variable antibody domain. Isolation and folding of the variable part of the antibody is therefore simplified. This variable part of the monomeric camelid antibody is called a VHH (variable domain of heavy chain) [21] with a molecular weight of 12-15 kDa (Figure 2D). These fragments can be derived from alpaca's (Figure 3). The alpaca is immunized against one or more antigens[22]. Subsequently the lymphocytes are harvested and total RNA is extracted. The RNA is then used to construct a cDNA library which is PCR amplified and ligated into a M13 phagemid vector, such that VHHs are expressed as pIII protein fusions on the phage coat. VHHs are subsequently isolated after phage panning against immobilized target antigens.

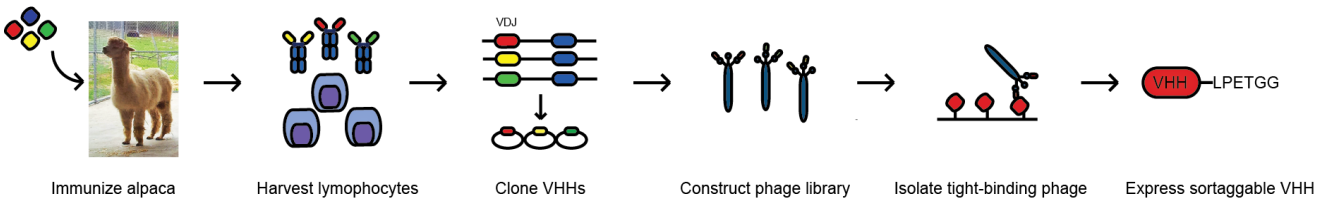

Figure 3: Production of single domain antibodies (VHHs).

When the sequences of the VHHs are known, they can also be sub-cloned into a bacterial expression vector. This allows expression on large scale and simple purification of VHHs.

VHH labeling

A well-developed technique to label VHHs is by sortagging[23-28]. This labeling method entails the modification of proteins by a chemoenzymatic reaction catalyzed by Sortase A. This technique is used for the labeling of proteins with fluorophores or other probes. Sortase A is an enzyme from the peptidase family C60 and found in *Staphylococcus aureus*[29]. This bacteria applies this enzyme for linking surface proteins to the bacterial cell wall. The enzyme recognizes the motif LPETG. The center of the active site of this protein contains cysteine which attacks the carbonyl of the threonine of the LPETG forming a tetrahedral intermediate. After reconfiguration, the glycine with His-tag leaves, forming the stable covalent thioacyl intermediate. Subsequently a nucleophilic substrate with probe containing multiple N-terminal glycines (at least three) attacks resulting in the VHH-label complex regenerating Sortase A.

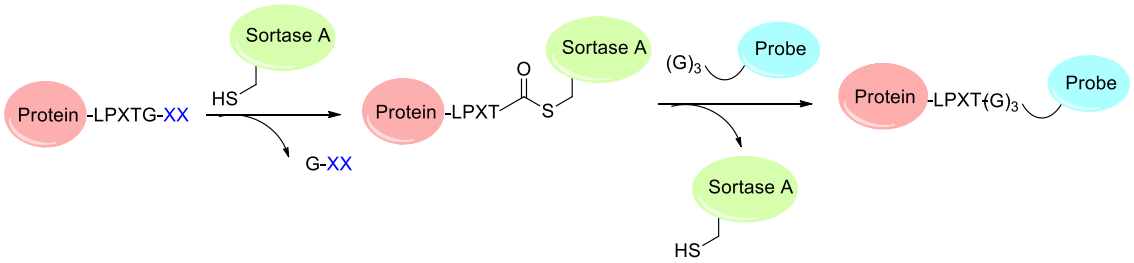

Figure 4: Sortagging: chemo enzymatic labeling of a protein by Sortase A.

This convenient labeling method allows the addition of any label of choice with N-terminal triglycine to proteins. Appending fluorophores or radioactive compounds to VHHs enables biological evaluation but also other probes can be attached to increase their functionality. These probes consists of biological material like (unnatural) amino acids and can therefore be synthesized by peptide chemistry.

Solid-phase peptide chemistry.

The peptide bond is the chemical bond between a carboxyl of one amino acid with the amino group of another amino acid. When brought together, these groups do not react spontaneously so nature uses enzymes to catalyze this process. In peptide synthesis, this process is performed by a series of robust chemical reactions without the use of enzymes[30]. There are two ways of synthesizing peptides: Solid phase peptide synthesis and liquid phase peptide synthesis. Liquid phase peptide synthesis is the synthesis of the peptide bond in an aqueous solution. This method is not applied very often anymore and is mainly replaced by solid phase peptide synthesis (Figure 5)[31].

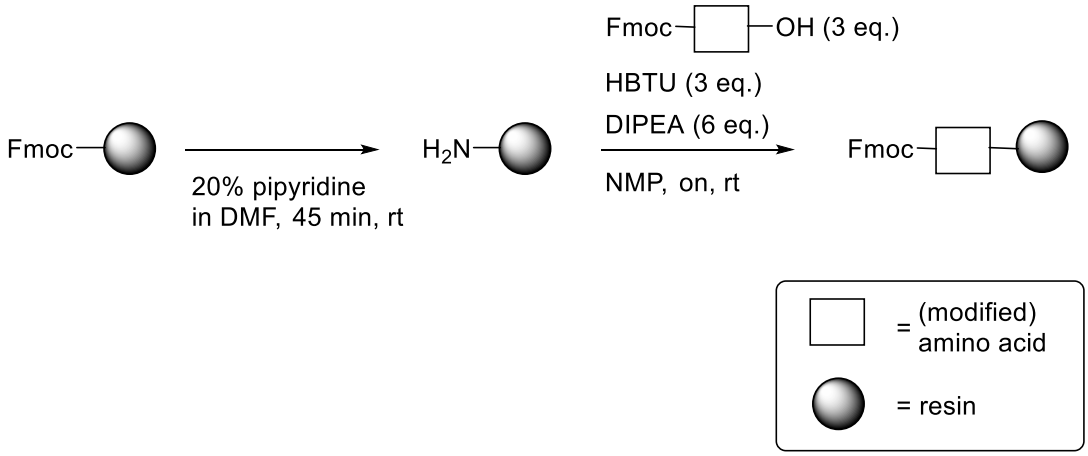

Figure 5. Addition of an fmoc-protected amino acid to a resin by solid phase peptide synthesis. These steps can be repeated to develop peptide chains or even small protein.

The solid phase is represented by resin beads. These beads are made from a porous synthetic material and have linkers on them with boc- or fmoc-protected N-terminal amino groups. Boc solid phase peptide synthesis has shown more problems with aggregation and more toxic chemicals have to be used[32]. Therefore fmoc solid phase peptide synthesis is applied more often[33]. The resin beads can be activated by 20 % pipyridine in DMF since fmoc is unstable in a basic environment. Subsequently an fmoc protected amino acid can be added to the resin by using (2-(1H-benzotriazol-1-yl)-1,1,3,3-tetramethyluronium hexafluorophosphate (HBTU) as an activating agent. To make sure the amino group is deprotonated, *N*,*N*-Diisopropylethylamine (DIPEA) is added for establishing a basic environment. Several washing steps to remove starting material and solvents result in the isolated fmoc protected amino acid connected to the resin in up to 99 % yield. This process can be repeated for adding more amino acids to synthesize small peptide chains or even small proteins. The chains have to be removed from the resin to finalize the peptide synthesis. Because the linker is unstable in an acidic environment, the peptide chain is disconnected from the resin with 90 % TFA in water.

Besides the development of natural amino acid chains or small proteins, this robust synthesis method can be applied in many more synthetic processes. The requirements for incorporation of compounds are:

- Stability in basic environment to prevent issues during deprotection.
- Contain an fmoc protected amino group and an acid group in not too close proximity.

The requirements for this simplifies the synthesis of peptides with unnatural side chains. This process is an eminent way of synthesizing linkers for protein modification.

The synthesis of long peptide chains can take a few days up to weeks. Recently machines have been developed for automation of this technique[34]. Since the machines can work more accurately and efficiently than humans, even overnight synthesis of small peptide chains has been accomplished. During this project a linker was developed by peptide chemistry which enabled chemical dimerization of VHHs.

Dimerization hypothesis

Previous studies have shown successful expression and functionality of genetically fused dimers of VHHs[35,36]. These dimers have better binding affinity for their receptor compared to their corresponding monomer. Although no direct issues have been reported, is hard to estimate the exact consequence for the folding and the performance of the individual VHHs of a dimer. In this project was elaborated on a chemical dimerization approach to connect two fully functional and properly refolded proteins. Because the binding capacity of both the VHHs would be truly equivalent, this dimer would be more comparable to full sized antibodies.

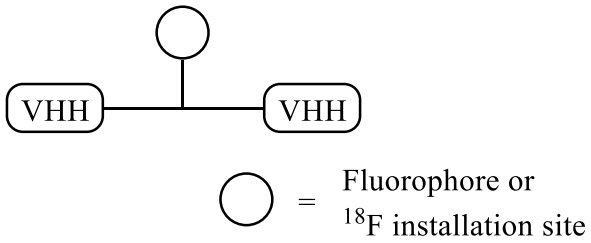

Figure 6. Dimerized VHHs with conjugated fluorophore or ^{18}F installation site

Peptide chemistry could be used to synthesize a linker which enables the connection of two VHH and a fluorophore for imaging or an installation site for ^{18}F. The fluorophore and ^{18}F enables biological analysis and quantification of binding affinities. The C-terminal LPETG motif on both the VHHs can be used for connecting the VHHs to avoid the blockage of the binding sites[37]. First a VHH with two biorthogonal handles was developed and subsequently perform click chemistry with another VHH to complete dimerization.

This chemical dimerization was applied on four different VHHs: VHH7, DC8 and DC15 which bind the MHC II complex on immune cells and DC13 which binds CD11b on myeloid cells such as neutrophils and dendritic cells. Evaluation of the labeled monomers and dimers provided an assessment of their binding affinity differences by analyzing with in *vitro* Fluorescence-activated cell sorting (FACS) and *in vivo* two photon imaging on spleen and lymph nodes. The final and main goal is to find VHH dimers which clearly show higher binding affinity and apply them in PET imaging.

Results and discussion

Design and synthesis of the dimer linkers

The expression of genetically fused VHH dimers in our lab has previously shown to be difficult because of incorrect folding and decreased solubility. Chemically dimerized VHH's with short linkers precipitated at 4º C. Therefore the linker for our chemical dimerization strategy entails two polyethylene glycol parts to enhance hydrophilicity and flexibility (Figure 7). This linker also contains the nucleophilic triglycine group which is recognized by Sortase A and can be conjugated to a VHH with LPXTG motif. A second function of this linker is the cysteine located in the center. Cysteine reacts bioorthogonally with a maleimide group, making the addition of commercially available dyes-maleimides or TCO-malaimide convenient. The final group of the linker is a lysine-N_3 utilized for dimerization with another VHH functionalized with dibenzocyclooctyne group (DBCO).

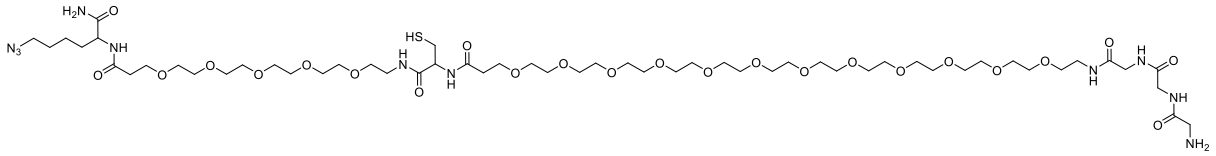

*Figure 7: Linker **1** synthesized by solid phase peptide chemistry containing an azide functionality, cysteine for convenient addition of fluorophores and triglycine for sortase A chemoenzymatic reaction with VHHs.*

Linker **1** was synthesized by standard solid phase peptide synthesis. The first attempts to perform the peptide synthesis by hand were unsuccessful since the coupling of fmoc-cysteine failed repeatedly. The first attempt using an automated peptide synthesizer yielded the linker efficiently. This peptide synthesizer utilizes fmoc solid phase peptide synthesis. The linker was purified by HPLC and the calculated mass was confirmed by LC-MS.

After obtaining linker **1**, the subsequent step is to add a dye to the linker used for the dimers for analyzing with FACS and two-photon imaging. The coupling of cysteine to maleimide is highly specific and efficient[38]. Therefore Alexa647-maleimide and TexasRed-maleimide were simply conjugated to the linker in a basic aqueous environment resulting in the linker-dye constructs **2** and **3**. PET imaging requires the equipment of a radioactive compound on the linker. To accomplish that, first a trans-cyclooctene (TCO) moiety was introduced on the linker resulting in linker **4**. TCO allows us to add a tetrazine-functionalized radioactive tag.

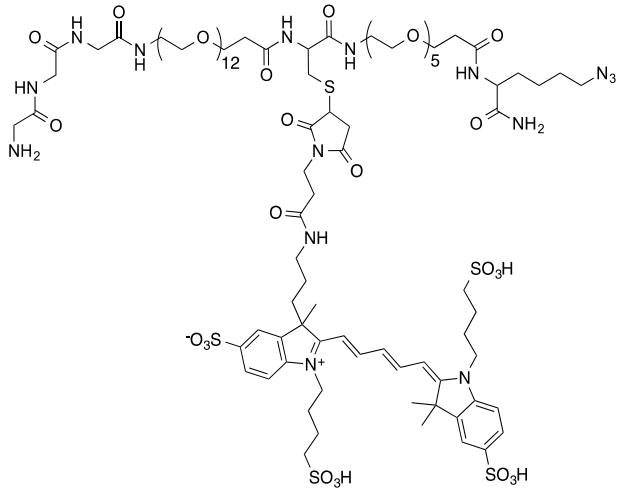

*Figure 8: Linker **2**; linker **1** functionalized with Alexa647 by the biorthogonal cysteine-maleimide reaction.*

Figure 8 shows the linker **1**–Alexa647 construct. The structure of Alexa647 is known, but the company does not provide the structure of Alexa647-maleimide. Therefore the exact structure of the linker used to connect Alexa647 and maleimide is not known. LC-MS showed the molar mass of the linker **1**-Alexa647 construct to be 2318.4 $g \cdot mol^{-1}$. From this value we were able to hypothesize about the structure of the Alexa647-maleimide. The Alexa647-labeled substrate was designed such that the reaction products could be used in FACS experiments to estimate relative *in vitro* binding affinities.

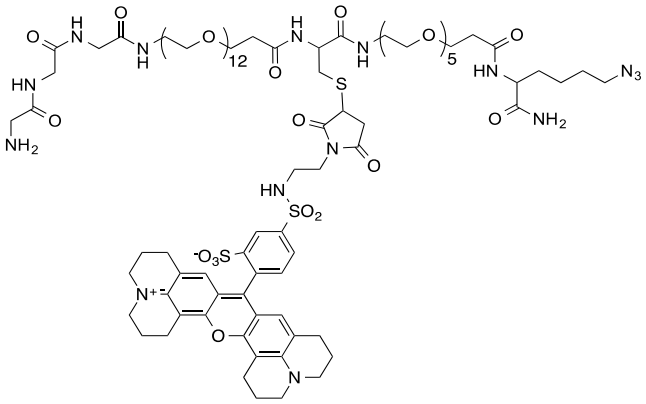

*Figure 9: Linker **3**; linker **1** functionalized with TexasRed by the biorthogonal cysteine-maleimide reaction.*

The linker-TexasRed construct **3** was synthesized the same way (Figure 9). TexasRed-maleimide is hydrophobic and therefore DMSO was added to the reaction mixture with the linker. The Texas Red-modified substrate was designed to enable two-photon microscopy and to estimate relative *in vivo* binding affinities.

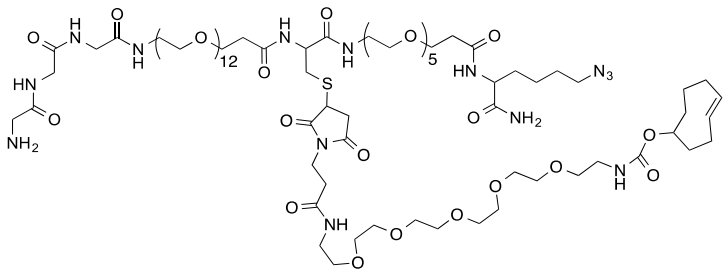

*Figure 10: Linker **4**; linker **1** functionalized with trans-cyclooctene by the biorthogonal cysteine-maleimide reaction.*

The TCO-modified substrate was produced to allow rapid installation of a tetrazine-functionalized radioactive tag for PET, in this case an isotopically labelled ^{18}F-labeled-tetrazine ($t_{1/2}$=110 min.) (Figure 10).

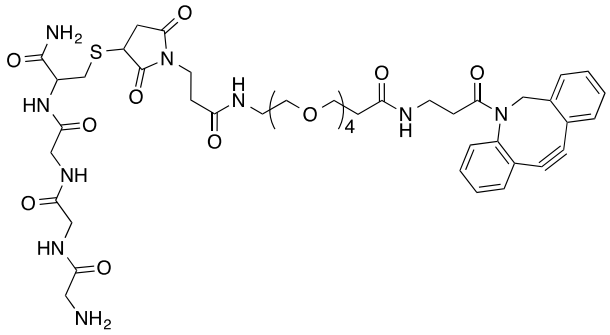

*Figure 11: Linker **5** containing triglycine for sortase A chemoenzymatic reaction with VHHs and DBCO for copper-free cycloaddition with azide functionalized VHHs.*

Linkers **2**, **3** and **4** contain an azide functionality and were appended to VHHs. For dimerization by a cycloaddition reaction another VHH was equipped with a dibenzylcyclooctyne (DBCO) functionality. Therefore linker **5** was synthesized with peptide chemistry, purified with HPLC and its structure was confirmed with LC-MS (Figure 11).

The single domain antibodies VHH7, DC8, DC15 and DC13 were labeled with linkers **2**, **3** and **4** in 70 to 90 % yield. Purification of labeled single domain antibodies after sortagging is usually performed by Ni-NTA/His-tag purification and subsequently separated based on their molecular weight by a PD-10 column. Sortase A, the byproducts of the sortagging and unlabeled VHHs contain His-tags. Therefore only the unreacted linkers and the labeled VHHs would remain after Ni-NTA/His-tag purification. The linkers and the single domain antibodies labeled with the linkers have a sufficient difference in molecular weight to be separated by this purification method, but after several attempts was clear that the labeled VHHs could not be purified this way.

The linkers **2**, **3** and **4** contain PEG moieties, which are very hydrophilic. In aqueous solution these linkers have a large hydrodynamic radius. Therefore the unreacted labels would elute from the column at the same time as the labeled VHHs. A more precise way of separating large molecules based on their weight is Fast Protein Liquid Chromatography (FPLC). In this size exclusion purification method the reaction mixture is injected in a large column which separated

the different components of the mixture based on the mobile phase and stationary phase. The mobile phase is usually an aqueous solution or a buffer and the stationary phase is composed of beads of cross-linked agarose. The mobile phase is kept constant, so the components are separated based on how fast they travel through the beads, which is linear with the molecular weight[40]. All of the labeled VHHs were purified easily with this method and confirmed by LC-MS (see experimental section). These constructs were used as labeled monomers to compare with the dimers during biological evaluation. Because both the mono- and bivalent derivatives contain a single mole of fluorophore per mole of construct, their binding strengths could be directly compared.

To functionalize the counterparts used for dimerization, the single domain antibodies VHH7, DC8, DC15 and DC13 were sortagged with the DBCO linker **5** in 80 – 90 % yield. In this case the linker did not have the same size of hydrodynamic radius as linkers **2**, **3** and **4** and showed therefore no overlap in elution time during purification by the PD-10 column. Because DBCO-functionalized VHHs did not show any color, the elution fractions had to be analyzed with a SDS-PAGE gel to know which fractions contained the product. Product formation and purification was confirmed by LC-MS.

Synthesis of the dimers

The labeled monomers with azide functionality were now ready for dimerization with the DBCO-functionalized VHHs. The copper free azide-DBCO click reaction was performed in 1 hour in PBS (Figure 12)[41]. This step was robust and showed 70 to 90 % yield for all the obtained dimers. The homodimers of the single domain antibodies VHH7, DC8, DC15 and DC13 and the heterodimer DC13-DC8 were synthesized. All of the dimers were purified by FPLC and product formation and purification was confirmed by LC-MS.

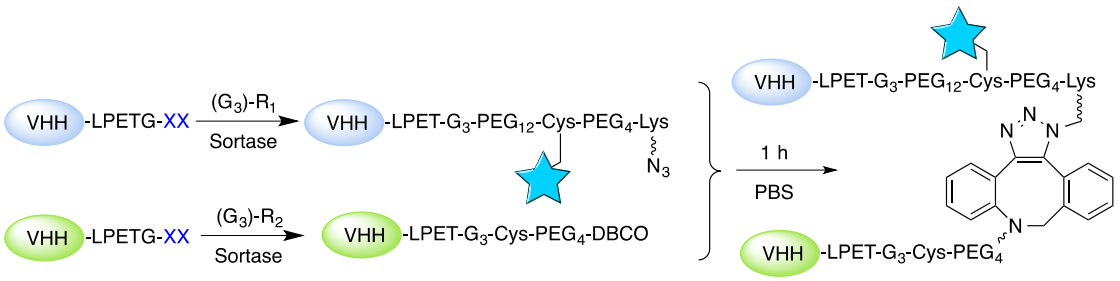

*Figure 12. Summary of the dimerization technique. First VHHs were sortagged with the linkers **2**, **3** and **4** containing the fluorophore or TCO and the azide functionality. The other VHH was sortagged with linker **5** containing the DBCO functionality. Eventually the dimerization was performed in 1 hour in PBS yielding the fluorophore or TCO labeled dimers.*

This dimerization technique has shown to be robust and reproducible with VHH7, DC8, DC15 and DC13. All the reactions proceeded rapidly and showed high yields. The dimers are stable at 4 ºC for over 48 hours but were usually kept at -80 ºC and didn't show precipitation possibly because of the long flexible and hydrophilic PEG linker.

The three functions of the linkers not only enables the convenient synthesizing of labeled dimers, but also the addition of other functionalities like large PEG moieties to VHHs. These PEG-tails could increase the half-life of VHHs in the bloodstream and therefore enhance staining abilities. Further research could show if the linkers could also be applied as a general tool for dual-labeling of VHHs and other proteins.

SDS-PAGE analysis

All confirmation of the VHH-constructs was done by LC-MS and the mass spectra are shown in the experimental section. To verify the purity, the constructs were loaded on a SDS-Page gel. Figure 13 shows the SDS-page gel of all the constructs of DC13.

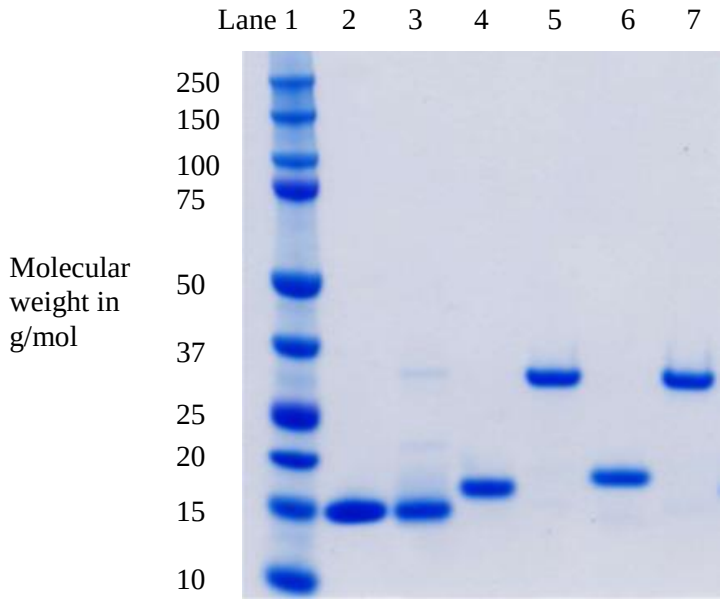

Figure 13: SDS-page gel of the DC13 constructs.

Lane 1 represents the marker from 10 to 250 g/mol. The smallest construct is unlabeled DC13 shown in lane 2. The third lane shows DC13 sortagged with linker **5** (DC13-DBCO). Lane 4 represents DC13 sortagged with TexasRed linker **3** (DC13-TexasRed-azide). The dimer of DC13-DBCO and DC13-TexasRed-azide is shown in lane 5. Lane 6 represents DC13 sortagged with Alexa647 linker **2** (DC13-Alexa647-azide). And finally lane 6 shows the DC13 dimer labeled with Alexa647. All the values of the masses shown in this SDS-Page gel correspond with the values obtained with LC-MS (see experimental section).

FACS

In order to evaluate the difference in receptor affinity *in vitro* between the dimers and monomers of VHH7, DC8, DC13 and DC15 labeled with Alexa647 were analyzed by FACS experiments.

VHH7, DC8 and DC15 bind MHC Class II. Therefore 10^6 splenocytes from a GFP-MHC II knock in mouse were stained with different concentrations of monomers and dimers and analyzed by FACS. Populations were gated on live, GFP+ cells, and the mean Alexa647 fluorescence of each population is plotted. The mean fluorescence corresponds to the binding affinity of the VHH for its target. The higher the mean fluorescence, the higher the binding affinity. Figure 14 shows the difference in binding affinity for VHH7-dimer and VHH7 monomer. The x-axis shows the VHH concentration in nM and the y-axis shows the percentage of the maximal fluorescence detected at the highest VHH concentrations. Decreasing the concentration resulted in less staining of the splenocytes. Comparing the two graphs we see that VHH7 monomer shows substantial decrease in staining at 100 nM but VHH7 dimer still shows maximal staining. Lower concentrations also indicate that the binding affinity of VHH7-dimer is enhanced compared to VHH monomer.

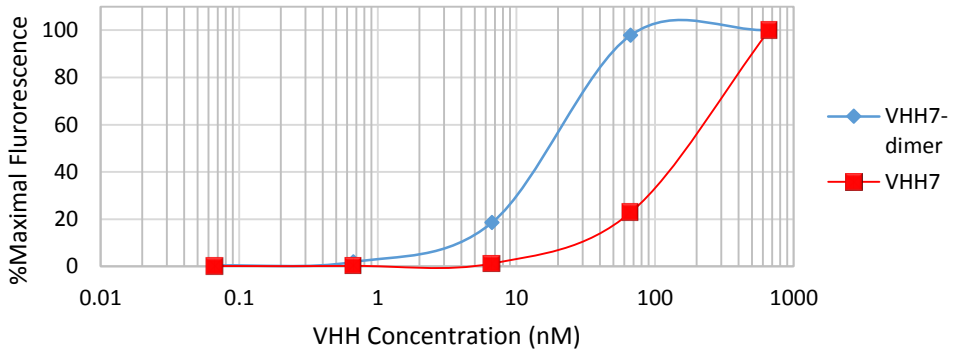

Figure 14: Mean fluorescence of the stained splenocytes from a GFP-MHC knock in mouse plotted against different concentrations of DC8 monomer and dimer.

Previous research has shown that DC8 monomer binds MHC Class II better than VHH7[15]. 10^6 splenocytes from a GFP-MHC knock in mouse were stained with DC8 monomers and dimers. The cells were analyzed with FACS and populations were gated on live, GFP+ cells, and the mean Alexa647 fluorescence of each population is plotted. Where VHH7 monomer showed no staining at 100 nM, the DC8 monomer still stains at this concentration. DC8 dimer shows still binding of MHC Class II at 10 nM (Figure 15). This shows conformity to our hypothesis that the examined VHH dimers have increased affinity for their target compared to VHH monomers.

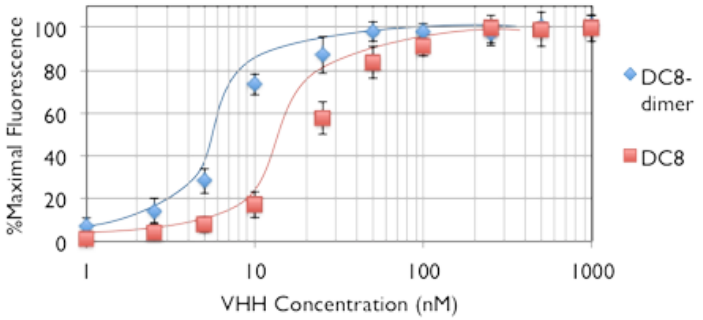

Figure 15: Mean fluorescence of the stained splenocytes from a GFP-MHC knock in mouse plotted against different concentrations of DC8 monomer and dimer.

Since DC13 targets CD11b, the staining experiment with DC13 required CD11b^{+} mutuDC dendritic cells. These cells expressed enough CD11b to compare affinity differences between DC13 monomer and DC13 dimer. The cells were stained and analyzed with FACS. Populations were gated on live single cells, and the mean Alexa647 fluorescence of each population is plotted. DC13 dimer binds more efficiently to its target than DC13 monomer (Figure 16).

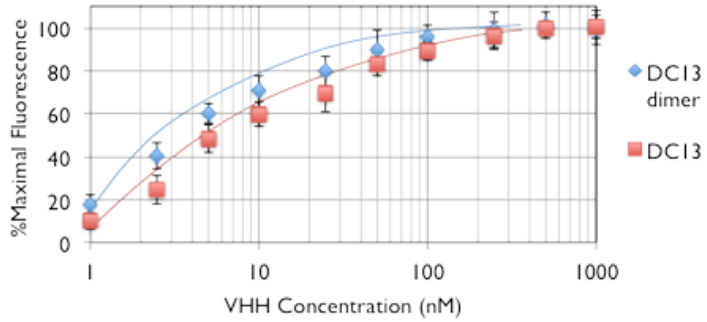

Figure 16: Mean fluorescence of the stained CD11b^{+} mutuDC dendritic cells plotted against different concentrations of DC13 monomer and dimer.

Finally DC15 monomer and dimer were compared. DC15 binds to MHC Class II so the staining experiment was performed with splenocytes from a GFP-MHC Class II knock in mouse. The cells were analyzed by FACS and populations were gated on live, GFP+ cells, and the mean Alexa647 fluorescence of each population is plotted. DC1-dimer binds better to MHC class II than DC15 monomer but the difference in binding affinity between DC15-dimer and DC15 monomer is smaller compared to the other VHHs binding MHC Class II (Figure 17).

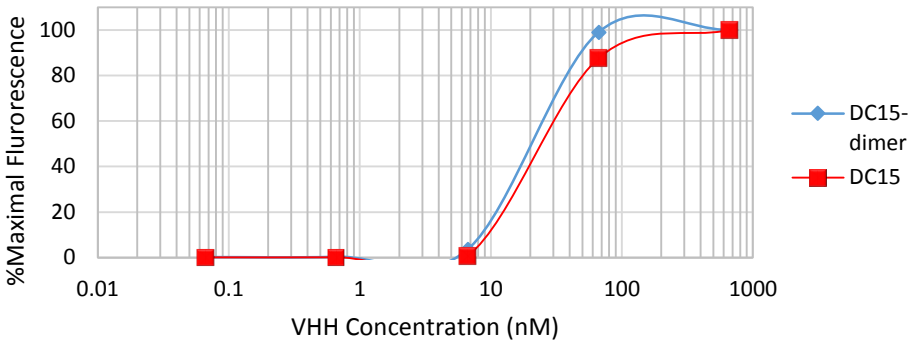

Figure 17: Mean fluorescence of splenocytes for different concentrations of DC15

These FACS results indicate that the dimers, except for DC15, bind their target about 3 to 5 times better than their corresponding monomers. These experiments gave a clear assessment of which monomers and dimers would be interesting for PET imaging experiments. To give a better insight in which VHH monomers and dimers were suitable for subsequent *in vivo* evaluation with PET imaging, first *in vivo* two photon imaging was performed.

In vivo evaluation with Two-photon imaging

In vitro evaluation with FACS experiments gave us insight in the relative binding affinities of the monomers and dimers. To confirm these results, VHH dimers and monomers sortagged with TexasRed were analyzed with Two-photon imaging. With these experiments the *in vivo* binding characteristics of the VHH dimers and monomers were analyzed. Therefore VHH7, DC8 and DC15 were sortagged with linker **3**. Because there is far more expression of MHC Class II on splenocytes compared to that of CD11b, only the binding affinities of the VHHs which bind MHC Class II are explored.

Mice were injected i.v. with equal amounts of monomers and dimers (0.25 nmol) of VHH7, DC8 or DC15. Two hours after injection the mice were euthanized and the spleen and lymph nodes were excised for examination by two photon microscopy. This technique is based on the idea that two photons with lower energy can excite a fluorophore in a similar fashion as one photon with high energy. Therefore the excitation of a fluorophore by a special laser using red-shifted excitation light results in the emission of a fluorescent photon which is at higher energy than the photons used for excitation. This results in less damaging of the sample, efficient light detection and lower background. This technique can be used for imaging living tissue up to about 1 millimeter in depth[42].

Figure 18 shows the difference in staining pattern in the spleen between the VHH7 monomer compared to the dimer. The intensity of the red color represents the amount of staining. This demonstrates that the VHH7 dimer stains better than its corresponding monomer which is in accordance with our FACS results. Figure 19 shows the difference between the DC8 monomer and dimer. A similar pattern is visible verifying that also the DC8 dimer stains better than DC8 which is also in conformity with the FACS results. The different staining pattern of DC15 monomer and DC15 dimer is shown in Figure 20. The difference between the DC15 monomer and dimer is less visible, yet the staining intensity of the dimer is clearly enhanced in local areas compared to the monomer. The examined VHH dimers clearly show enhanced staining of splenocytes compared to their corresponding monomer.

VHH7 Monomer VHH7 Dimer

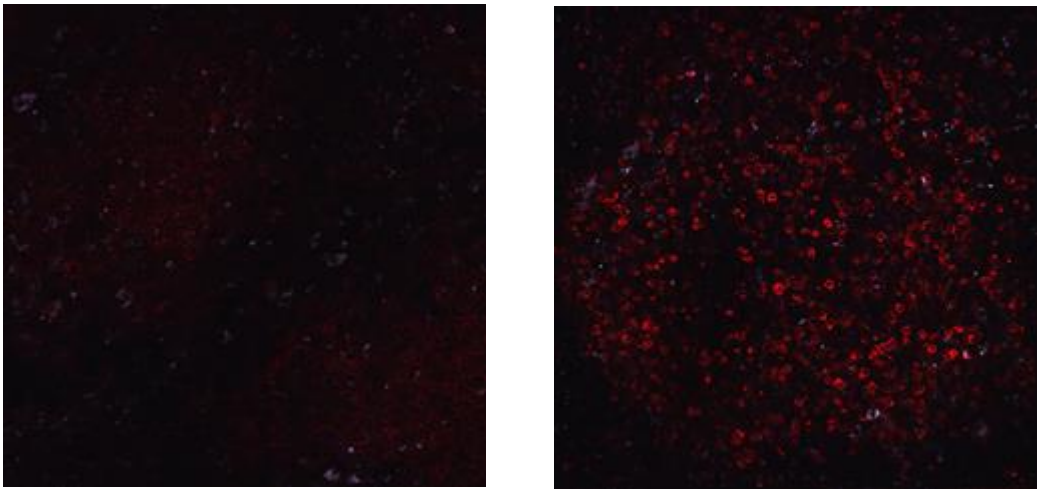

Figure 18: Different staining patterns on spleen for VHH7 monomer and dimer

DC8 Monomer

DC8 Dimer

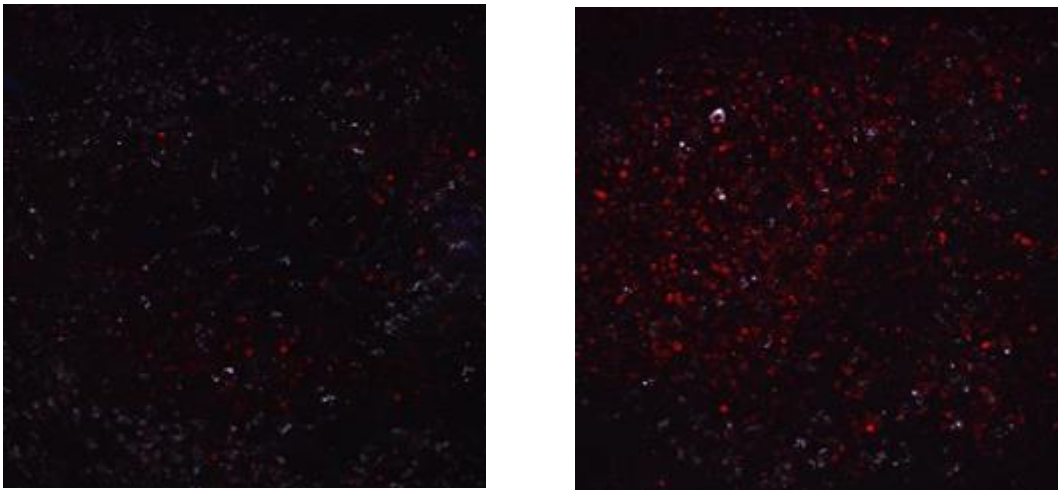

Figure 19: Different staining patterns on spleen for DC8 monomer and dimer

DC15 Monomer

DC15 Dimer

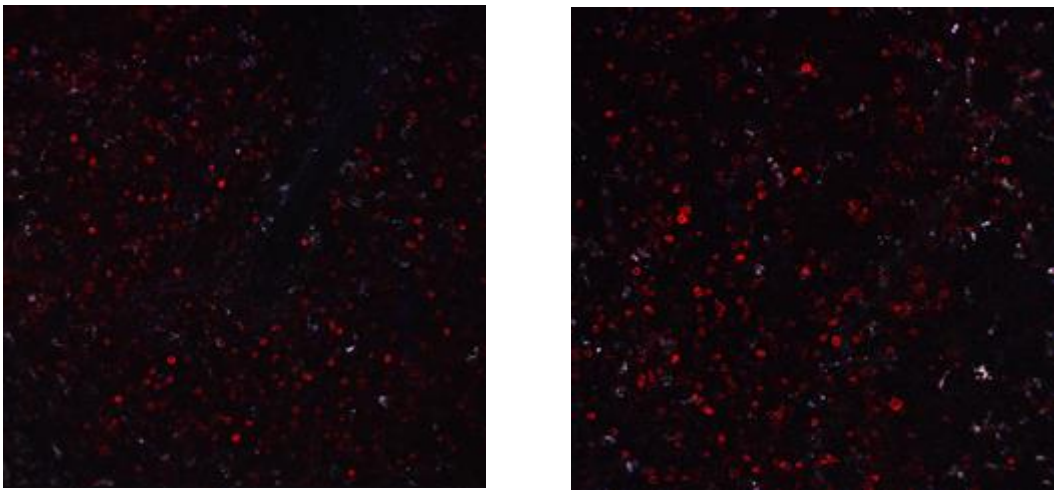

Figure 20: Different staining patterns on spleen for DC15 monomer and dimer

Similar results are shown at the staining pattern of the lymph nodes. Because there are less MHC Class II positive cells in the lymph nodes compared to the spleen, the staining with VHH targeting this receptor is less clear. The blue color showing in the lymph nodes represents collagen.

Contrary to the VHH7 monomer, the VHH7 dimer stained the lymph nodes well at this concentration (Figure 21). For DC8 monomer and dimer the difference is similar and (Figure 22) again the difference in staining pattern between DC15 monomer and dimer is not clear, but local areas showed qualitatively enhanced staining (Figure 23).

VHH7 Monomer

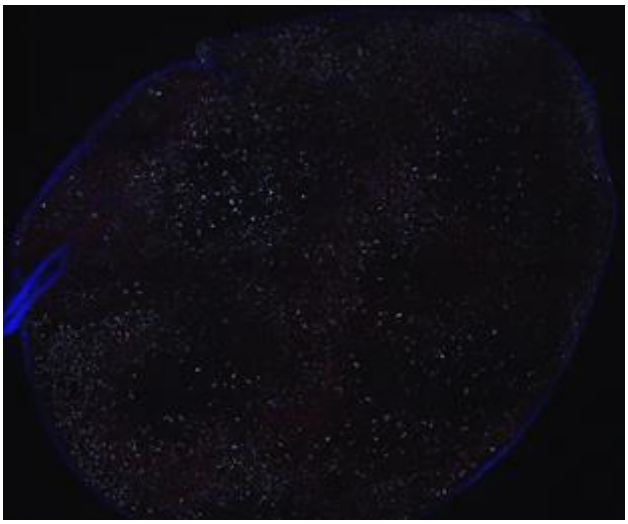

VHH7 Dimer

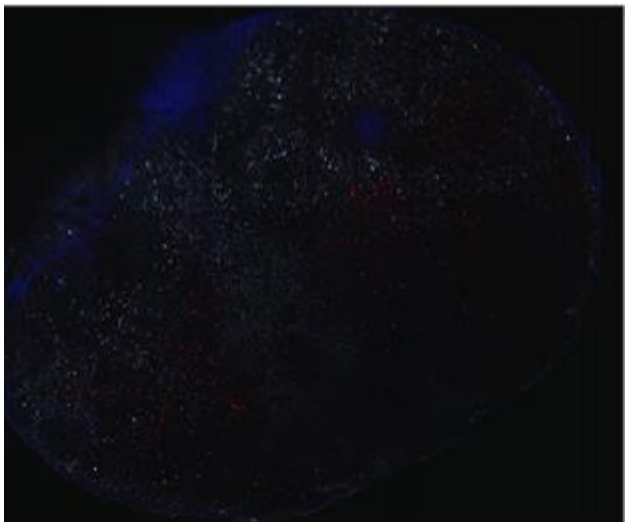

Figure 21: Different staining patterns on lymph nodes for VHH7 monomer and dimer

DC8 Monomer

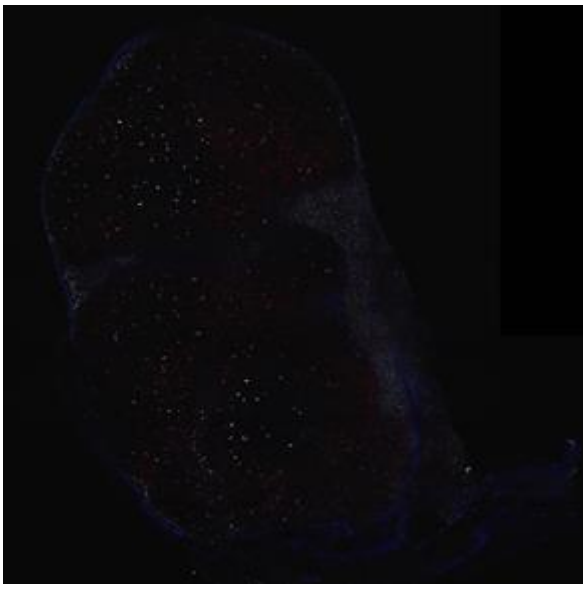

DC8 Dimer

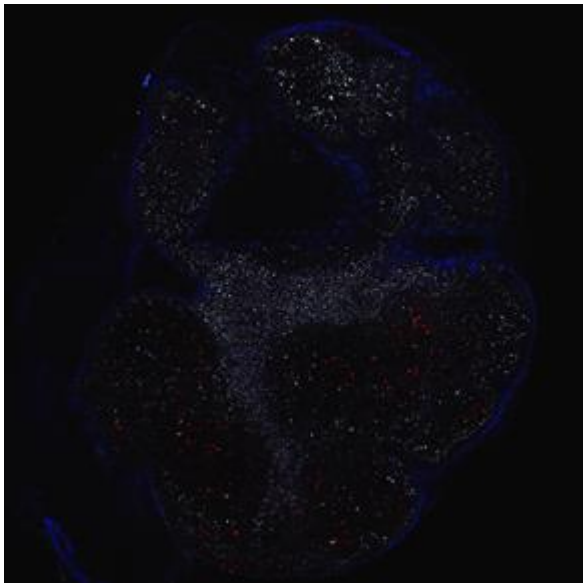

Figure 22: Different staining patterns on lymph nodes for DC8 monomer and dimer

DC15 monomer

DC15 dimer

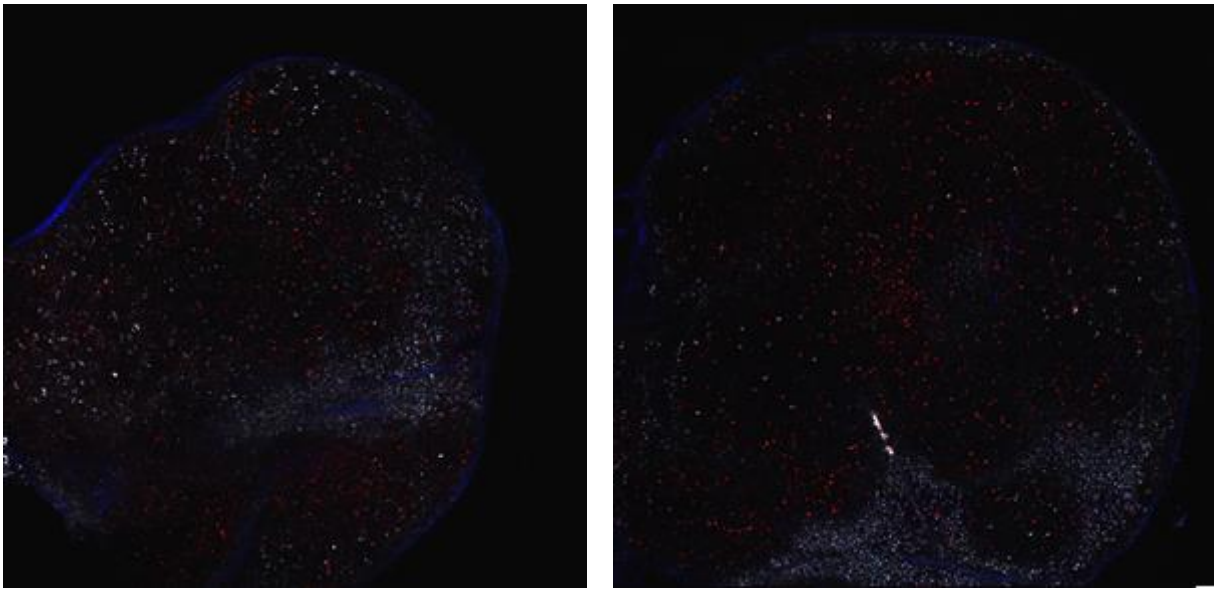

Figure 23: Different staining patterns on lymph nodes for DC15 monomer and dimer

PET imaging

The final aim is to demonstrate that the dimers could be used in *in vivo* PET imaging. VHHs sortagged with linker **5** have a TCO moiety, which was used for further modification with ^{18}F-tetrazine. Appending a radioactive compound on the dimers enables the *in vivo* evaluation with PET imaging. Because there was no time left during this project, later my supervisor (Mohammad) did PET imaging with the DC13-dimer and DC8 dimer. This paragraph shows the possibilities of PET imaging to detect immune cells and tumor cells in mouse.

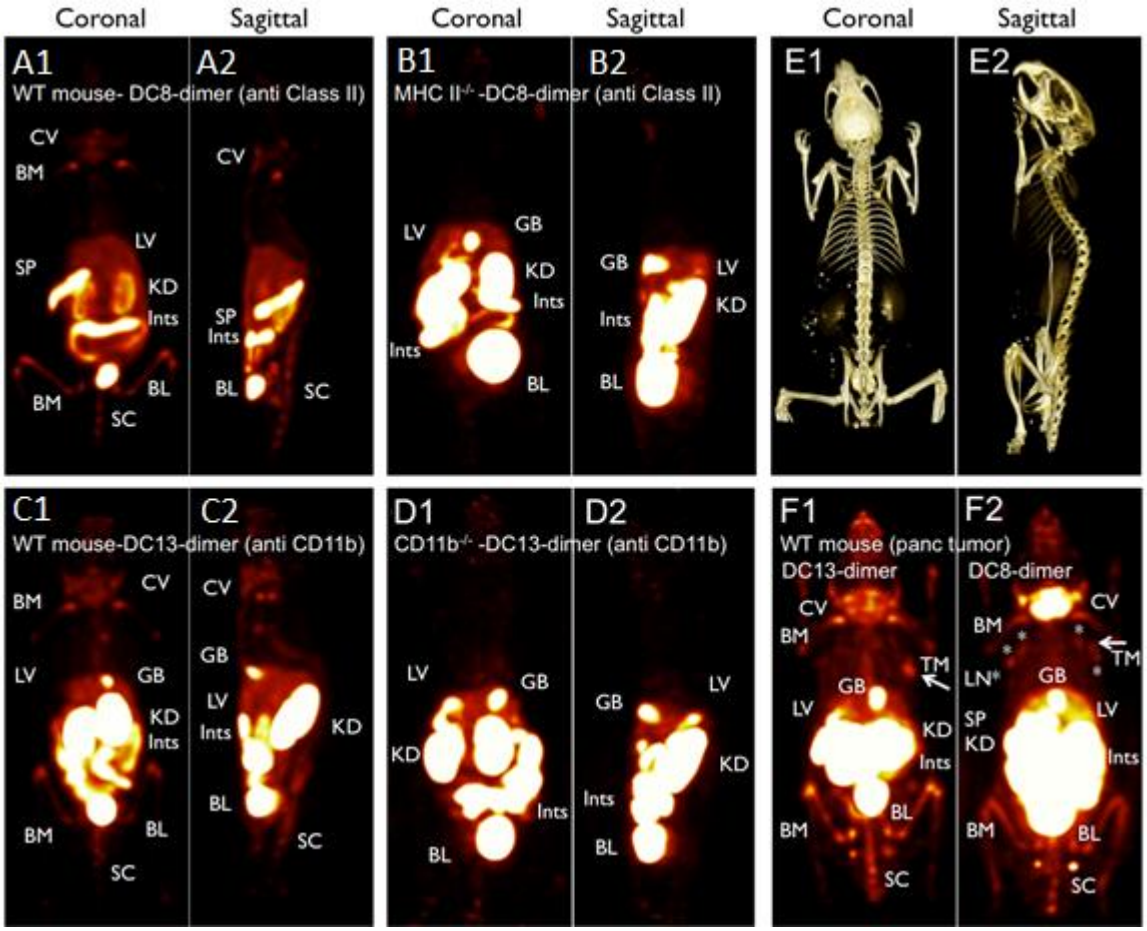

Figure 24. PET imaging of A) WT mouse injected with DC8-dimer, B) MHC II $^{-/-}$mouse injected with DC8-dimer, C) WT mouse injected with DC13-dimer, D) CD11b$^{-/-}$ mouse injected with DC13-dimer. F) WT mouse with inoculated subcutaneously pancreatic tumor injected with F1) DC13-dimer and F2) DC8 dimer. Letters indicate: SP: Spleen CV: cervical lymph nodes; BM: bone marrow; GB: gallbladder; LV: liver; KD: kidneys; Ints: intestines; BL: bladder; SC: spinal cord

WT, MHC II$^{-/-}$ and CD11b$^{-/-}$ mice MHC were injected with ^{18}F-labeled dimers of DC13 and DC8 and subsequently analyzed with a PET scan. Because DC8-dimer binds to the MHC Class II complex, the immune cells are visible. WT mouse injected with DC8-dimer clearly shows the lymphoid organs: bone marrow, cervical lymph nodes and spleen. In WT mouse injected with DC13-dimer also the lymphoid organs are visible. These organs are not visible in MHC II$^{-/-}$ and CD11b$^{-/-}$ mice, indicating the DC8-dimer specifically bind to the MHC II^{+} organs and the DC13-dimer specifically to CD11b^{+} organs. The intensity of the signal in spleen is lower than that of MHC II, as CD11b protein has much lower expression level on splenocytes compared to MHC II protein.

Since tumors are infiltrated by immune cells, the dimers could also be used for imaging of tumors in mice. Mice subcutaneously inoculated with pancreatic cancer cells were imaged after two weeks. The arrows are pointing at the tumors and in F2 the lymph nodes are indicated with stars. This PET imaging confirmed that the tested dimers bind to immune cells and could be used for imaging of an immune response or tumor detection.

Conclusion

During this project an efficient and robust strategy for the coupling of two VHHs with a fluorophore or radioactive compound is developed. The linkers used in this method is easily obtained with solid phase peptide chemistry. This linker contains the motif Gly3 and could therefore be installed on one VHH. These linkers enable the VHH to connect bioorthogonally both with another VHH and with a fluorophore or radioactive compound. The obtained dimers are stable and show full functionality.

Dimers and monomers labeled with Alexa647 were subsequently compared by FACS. The dimers show ~3-5-fold better binding affinities for their receptor than the monomers based on the concentration required for half-maximal binding. *In vivo* two photon imaging confirmed this by showing more intense staining with dimers than monomers. Binding affinity differences obtained from these experiments gave an assessment for which VHHs could be used for PET imaging. PET imaging later performed by Mohammad with monomers and dimers of DC8 and DC13 showed staining of lymph nodes and spleen, as expected, further confirming the FACS and two photon results.

This strategy has provided more information about single domain antibodies and could trigger further research with dimers. The developed linkers also enable the dual-labeling with proteins containing a LPETG motif and could therefore also be applied in VHH labeling and other protein analysis experiments.

Experimental section

Synthesis of $(Gly)_3$-PEG_4-Cys(TCO)-PEG_{11}-Lys(azide).

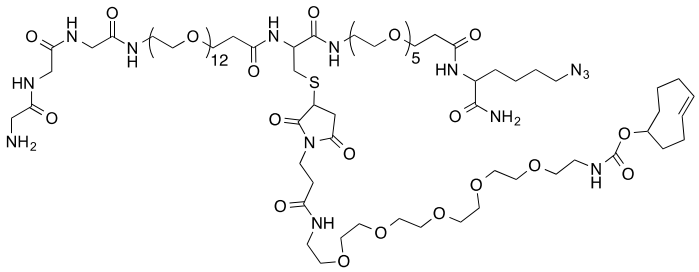

The peptide $(Gly)_3$-PEG_4-Cys-PEG_{11}-Lys(azide) was synthesized by standard solid phase peptide synthesis. Maleimide-TCO (from Conju-bio) was dissolved in 0.05 M $NaCO_3$ buffer pH 8.3. The peptide was added and left to stir at room temperature for 1 h until LC-MS indicated near-complete conversion to the product. The solution was filtered and purified by reverse phase-HPLC with a semi-preparative column (Phenomenex, C_{18} column , Gemini, 5 µm, 10x250 mm) at a flow rate of 5.0 mL/min.; solvent A: 0.1% TFA in H_2O, solvent B: 0.1% TFA in CH_3CN. Product eluted at 30–35% solvent B. Fractions containing pure product were collected and lyophilized. LC-MS calculated for $C_{83}H_{151}N_{14}O_{34}S$ $[M+H]^+$ 1920.0, found 1919.0.

Synthesis of $(Gly)_3$-PEG_4-Cys(Texas Red)-PEG_{11}-Lys(azide).

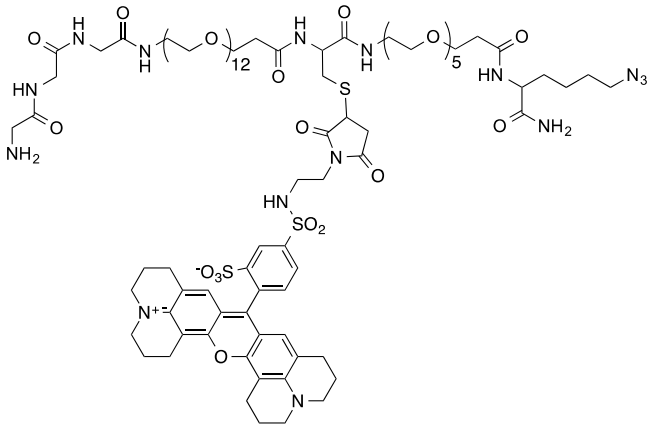

The peptide $(Gly)_3$-PEG_4-Cys-PEG_{11}-Lys(azide) was synthesized by standard solid phase peptide synthesis and was dissolved in 0.05 M $NaCO_3$ buffer pH 8.3. Maleimide-Texas Red (from Vector Labs) was dissolved in DMSO and then was added to the solution and left to stir at room temperature for 1 h until LC-MS indicated near-complete conversion to the product. The solution was filtered and purified by reverse phase-HPLC with a semi-preparative column (Phenomenex, C_{18} column, Gemini, 5 µm, 10x250 mm) at a flow rate of 5.0 mL/min.; solvent A: 0.1% TFA in H_2O, solvent B: 0.1% TFA in CH_3CN. Product eluted at 30–35% solvent B. Fractions containing pure product were collected and lyophilized. LC-MS calculated for $C_{92}H_{142}N_{15}O_{32}S_3$ $[M+H]^+$ 2064.9, found 2063.9.

Synthesis of $(Gly)_3$-PEG_4-Cys(Alexa647)-PEG_{11}-Lys(azide).

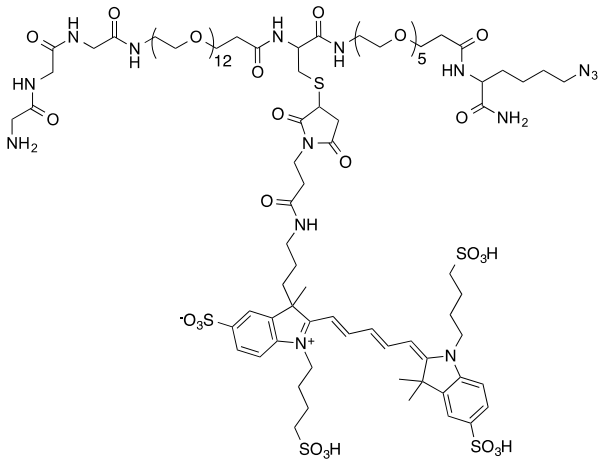

The peptide $(Gly)_3$-PEG_4-Cys-PEG_{11}-Lys(azide) was synthesized by standard solid phase peptide synthesis. Maleimide-Alexa647 (from Life Technology) was dissolved in 0.05 M $NaCO_3$ buffer pH 8.3. The peptide was added and left to stir at room temperature for 1 h until LC-MS indicated near-complete conversion to the product. The solution was filtered and purified by reverse phase-HPLC with a semi-preparative column (Phenomenex, C_{18} column, Gemini, 5 µm, 10x250 mm) at a flow rate of 5.0 mL/min.; solvent A: 0.1% TFA in H_2O, solvent B: 0.1% TFA in CH_3CN. Product eluted at 30–35% solvent B. Fractions containing pure product were collected and lyophilized. LC-MS calculated for $C_{97}H_{158}N_{15}O_{39}S_5$ $[M+H]^+$ 2317.9, found 2318.4.

Synthesis of (Gly)3-DBCO.

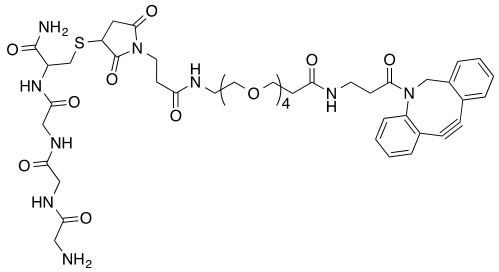

The tetrapeptide $(Gly)_3$-Cys was synthesized by standard solid phase peptide synthesis and was dissolved in 0.05 M $NaCO_3$ buffer pH 8.3. Maleimide-DBCO (from Click Chemistry Tools) was dissolved in DMSO and then was added to the solution and left to stir at room temperature for 1 h until LC-MS indicated near-complete conversion to the product. The solution was filtered and purified by reverse phase-HPLC with a semi-preparative column (Phenomenex, C_{18} column, Gemini, 5 µm, 10x250 mm) at a flow rate of 5.0 mL/min.; solvent A: 0.1% TFA in H_2O, solvent B: 0.1% TFA in CH_3CN. Product eluted at 35–40% solvent B. Fractions containing pure product were collected and lyophilized. LC-MS calculated for $C_{45}H_{60}N_9O_{13}S$ $[M+H]^+$ 966.4, found 966.4.

Enzymatic incorporation of substrates into proteins using sortase.

The penta-mutant sortase A, with an improved k_{cat}, was used[43]. Reaction mixtures (1 mL) contained Tris·HCl (50 mM, pH 7.5), $CaCl_2$ (10 mM), NaCl (150 mM), triglycine-containing probe (500 µM), LPETG-containing probe (100 µM), and sortase (5 µM)[44,45]. After incubation at 4 °C with agitation for 2 h, reaction products were analyzed by LC-MS. Yields were generally >90%. When the yield was below 90%, the reaction was allowed to proceed for an additional two hours, with addition of sortase to 10 µM and triglycine-containing probe to 1 mM. Ni-NTA beads were added to the reaction mixture with agitation for 5 min at 25 °C followed by centrifugation to remove sortase and any remaining unreacted His-tagged substrate. The final product was purified by size exclusion chromatography in PBS or Tris·HCl (50 mM, pH 7.5). The labeled protein was stored at -80 °C with 5% glycerol for up to six months.

Dimerization of VHHs.

The general procedure was as follows: the DBCO-VHH (1.3 eq, in PBS) was added to the azide-X-VHH (where X is either TCO, Texas Red or Alexa647) and the reaction was left to proceed at room temperature for ~1-3 hours with constant agitation, where LC-MS analysis revealed (generally) above 80% conversion to the corresponding dimer product. The final dimer product was purified via size exclusion chromatography (FPLC) using PBS as the eluting solvent.

LC-MS analysis of VHHs, their corresponding sortagged products and dimers.

VHH7 and its derivatives.

VHH7

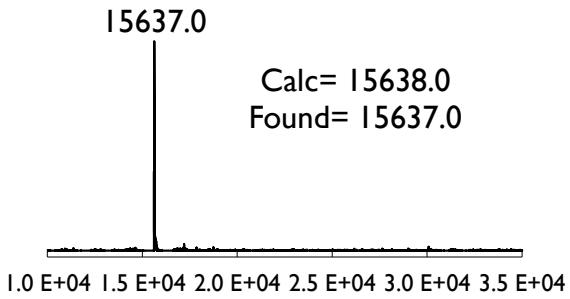

VHH7-DBCO

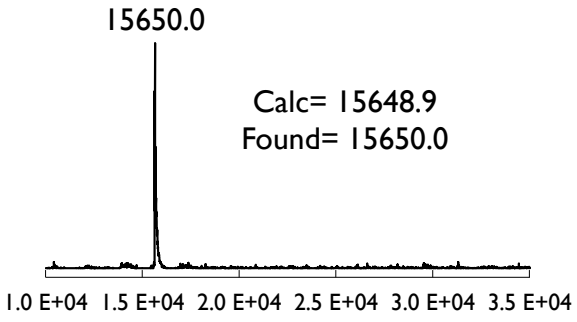

VHH7-azide-Alexa647

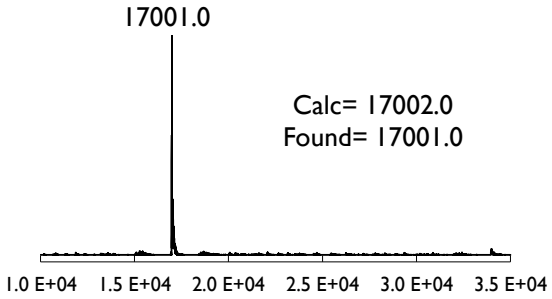

VHH7-VHH7-Alexa647 (homo dimer)

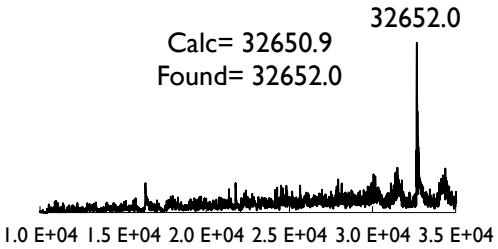

VHH7-azide-Texas Red

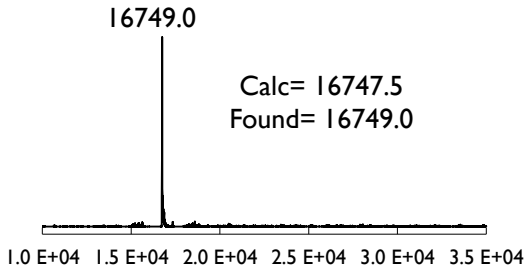

VHH7-VHH7-Texas Red (homo dimer)

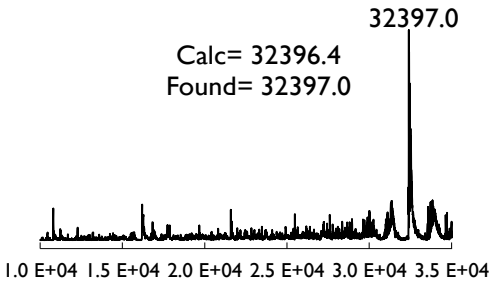

VHH7-azide-TCO

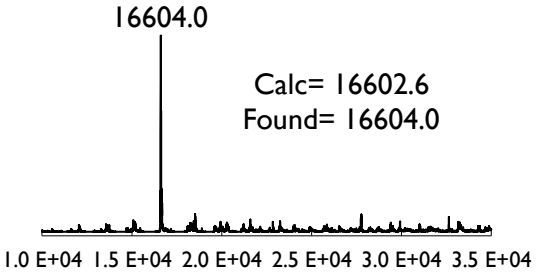

VHH7-VHH7-TCO (homo dimer)

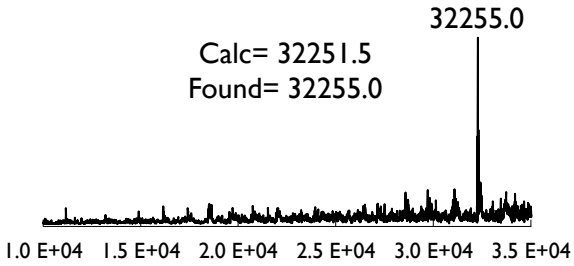

DC8 and its derivatives.

DC8

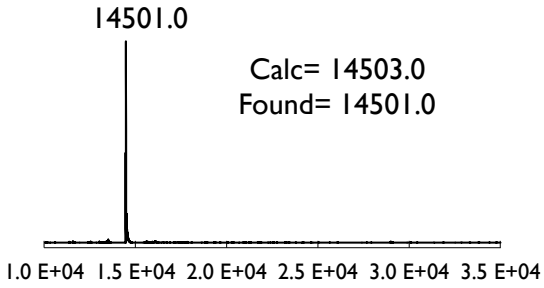

DC8-DBCO

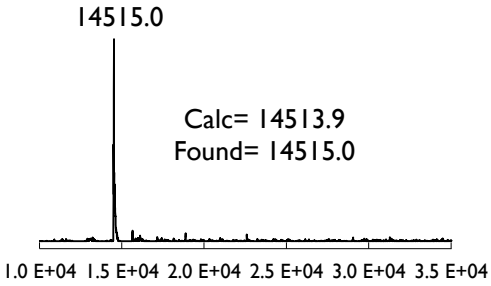

DC8-azide-Alexa647

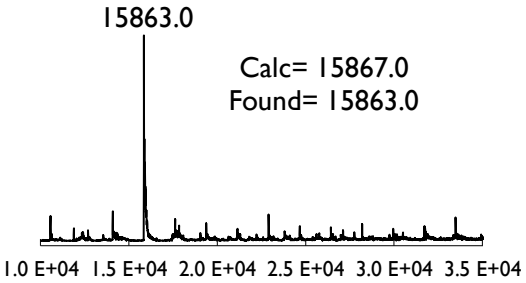

DC8-DC8-Alexa647 (homo dimer)

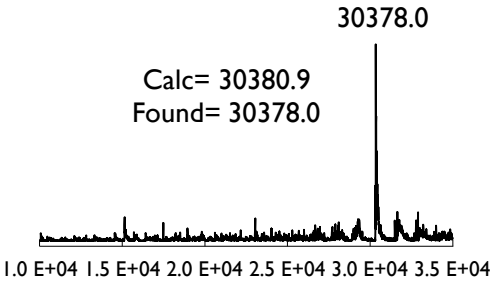

DC8-azide-Texas Red

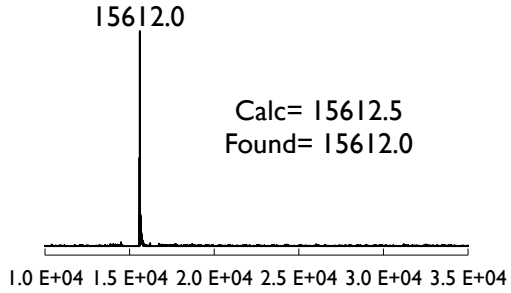

DC8-DC8-Texas Red (homo dimer)

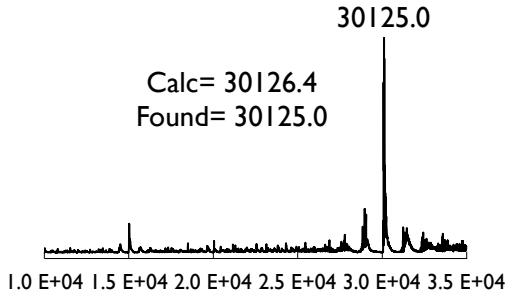

DC8-azide-TCO

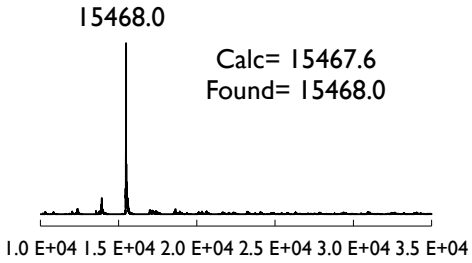

DC8-DC8-TCO (homo dimer)

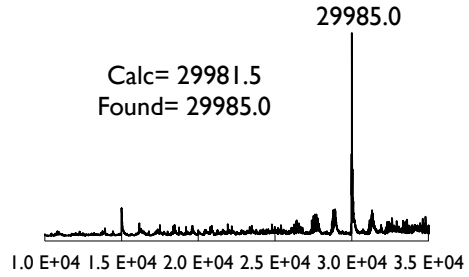

DC13 and its derivatives.

DC13

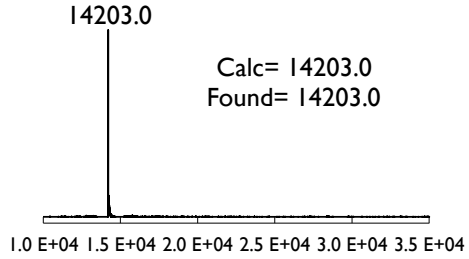

DC13-DBCO

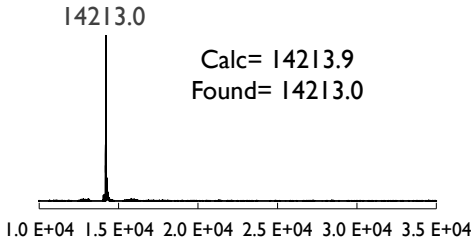

DC13-azide-Alexa647

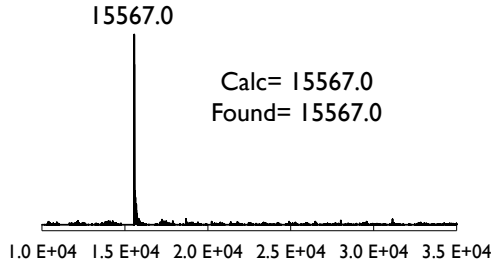

DC13-DC13-Alexa647 (homo dimer)

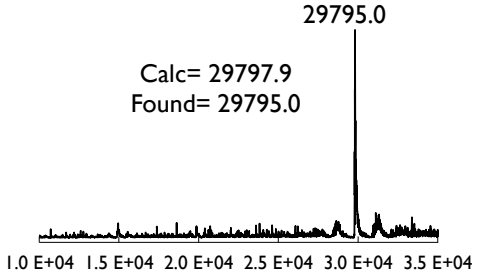

DC13-azide-Texas Red

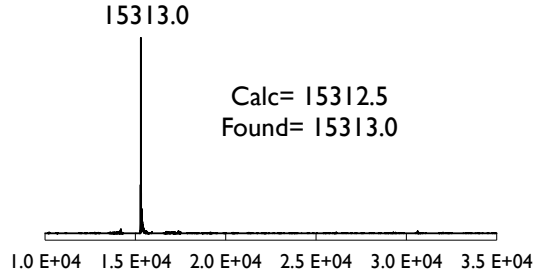

DC13-DC13-Texas Red (homo dimer)

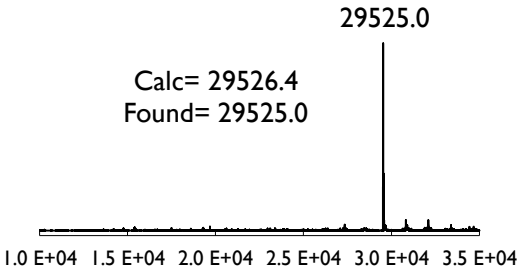

DC13-azide-TCO

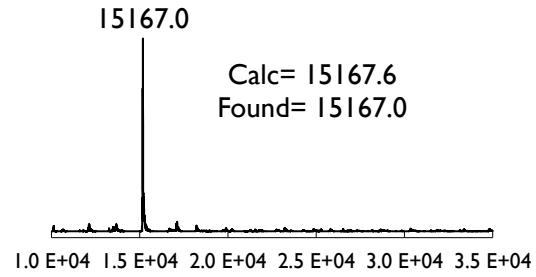

DC13-DC13-TCO (homo dimer)

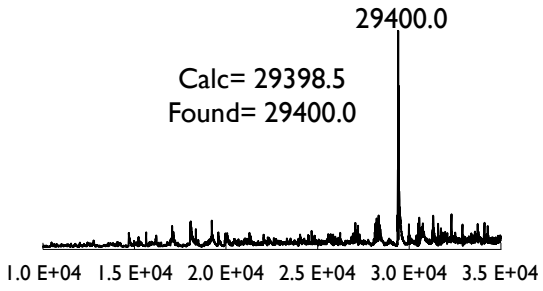

DC15 and its derivatives.

DC15

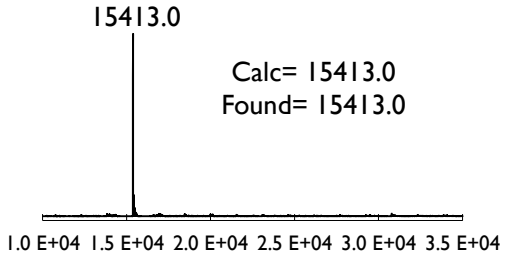

DC15-DBCO

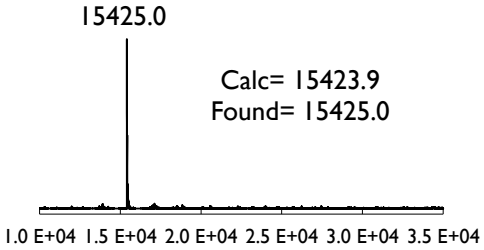

DC15-azide-Alexa647

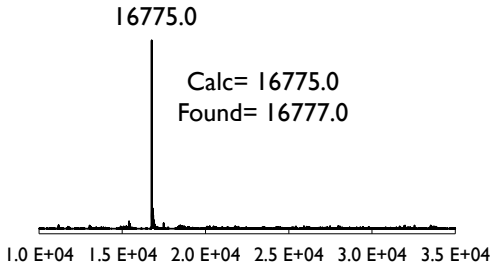

DC15-DC15-Alexa647 (homo dimer)

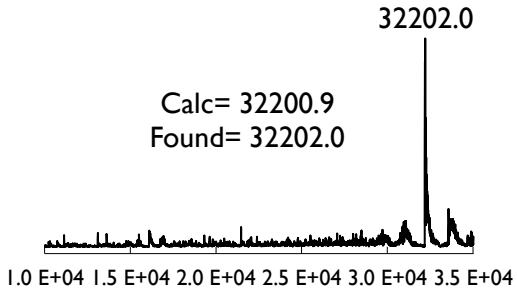

DC15-azide-Texas Red

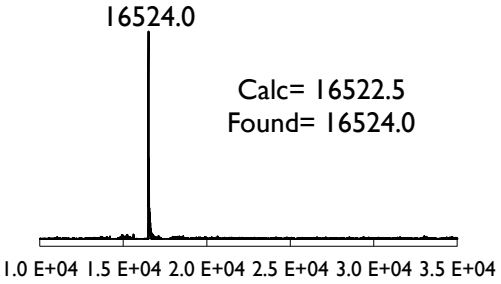

DC15-DC15-Texas Red (homo dimer)

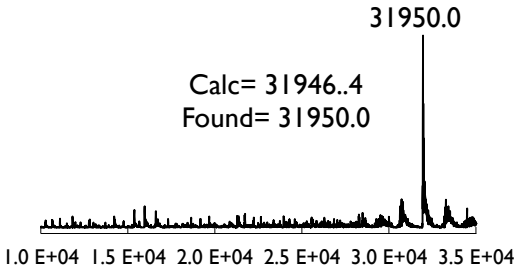

Two-photon imaging.

Two-photon imaging was performed with Olympus BX61 upright microscope (Olympus 25X 1.05 NA Plan Objective), fitted with a SpectraPysics MaiTai DeepSee laser. Images were acquired using 910 nm excitation and following filters; CFP (460-510), GFP (495-540) and a third filter (575-630) for the Texas Red signal. 2nd harmonics (collagen) were also detected in the CFP filter. Images were acquired with 5 µm Z resolution with Olympus FluoView FC1000 software. Tile images were saved as JPEG files. Images were processed to obtain a scale bar in Imaris v 7.4.0; no intensity or contrast adjustments were made.

Sequence of VHH7, DC8, DC13 and DC15

VHH7:
Nucleic Acid:
CAGGTGCAGCTGCAGGAGTCAGGGGGAGGATTGGTGCAGGCTGGGGACTCTCTGAGACT
CTCCTGCGCAGCCTCTGGACGCACCTTCAGTCGCGGTGTAATGGGCTGGTTCCGCCGGGC
TCCAGGGAAGGAGCGTGAGTTTGTAGCAATCTTTAGCGGGAGTAGCTGGAGTGGTCGTAG
TACATACTATTCAGACTCCGTAAAGGGCCGATTCACCATCTCCAGAGACAACGCCAAGAA
CACGGTGTATCTGCAAATGAACGGCCTGAAACCTGAGGACACGGCCGTTTATTACTGTGC
AGCGGGATATCCGGAGGCGTATAGCGCCTATGGTCGGGAGAGTACATATGACTACTGGG
GCCAGGGGACCCAGGTCACCGTCTCCTCAGGATCCCTTCCTGAAACTGGT

Peptide:
QVQLQESGGGLVQAGDSLRLSCAASGRTFSRGVMGWFRRAPGKEREFVAIFSGSSWSGRSTY
YSDSVKGRFTISRDNAKNTVYLQMNGLKPEDTAVYYCAAGYPEAYSAYGRESTYDYWGQG
TQVTVSSGSLPETGGHHHHHH

DC8:
Nucleic Acid:
CAGGTGCAGCTGCAGGAGTCAGGGGGAGGATTGGTGCAGCCTGGGGGGTCTCTGAGACT
CTCCTGTACAGCCTCTGGATTCACATTCAGTACTTACTACATGAGCTGGGTCCGCAAGGCT
CCAGGGAAGGGGCCCGAGTGGGTCTCAGTTATGAATAGTAGTGGTGGTGACACAAGGTA
TGCAGACTTCGTGAAGGGCCGATTCACCATCTCCAGAGACAACGCCAAGAACACACTGTA
TCTCCAAATGAACAGCCTGAAACCTGAGGATACGGCCCTGTATTACTGTGCGCAAGGTAG
ATCAGATATATACCCAACCTTCACGCGGGGCCAGGGGACCCAGGTCACCGTCTCCTCAGG
AGGACTGCCGGAAACCGGC

Peptide:
QVQLQESGGGLVQPGGSLRLSCTASGFTFSTYYMSWVRKAPGKGPEWVSVMNSSGGDTRYA
DFVKGRFTISRDNAKNTLYLQMNSLKPEDTALYYCAQGRSDIYPTFTRGQGTQVTVSSGSLPE
TGGHHHHHH

DC13:
Nucleic Acid:
CAGGTTCAACTGCAAGAGAGTGGCGGGGGCCTGGTTCAGACCGGTGGTTCTCTCCGGCTC
TCGTGTGCCGCAAGTGGAGTAGATTTTAACTGGTATAGCATGGGTTGGTTCAGGCAAGCC
CCTGGCAAAGAGCGGGAGTATGTGGCTTCGATTGACCAGGGAGGCGAGTTGGATTACGC
AATATCAGTAAAGGGCAGATTCACGATCTCCCGAGACAACGCGAAGAATATGGTGTATCT
CCAGATGAATTCGTTAAAGCCCGAAGACACCGCTGTATACTACTGTGCCGCAGATTTTTC
CGGCCGGGGTGCGTCAAACCCTGACAAGTATAAATATTGGGGACAGGGAACCCAAGTGA
CCGTCAGCAGCGGTGGGTTGCCCGAAACTGGAGGACACCATCACCATCACCAT

Peptide:
QVQLQESGGGLVQTGGSLRLSCAASGVDFNWYSMGWFR
QAPGKEREYVASIDQGGELDYAISVKGRFTISRDNAKNMVYLQMNSLKPEDTAVYYCAADFSGRGASNPDKYKYW
GQGTQVTVSSGGLPETGGHHHHHH

DC15:
Nucleic Acid:
CAGGTGCAGCTGCAGGAGTCAGGGGGAGGATTGGTGCAGCCTGGGGCGTCTCTGAGACT
CTCCTGCGTTTCTGCGTTCTCCTTAGATCATTATTCCGTAGCCTGGTTCCGCCAGGCCCCA
GGGAAGGAGCGTGAGGGGGTCTCATGTCACAGTCGGTCAAATAAAGCCACGGACTATGC
AGACTCCGTGAAGGGCCGATTCACCATCTCCAGAGACAGCGCCAAGCGCACGGTGTATCT
GCAAATGAACAACCTGAAACCAGAAGACACAGCCGTATATTACTGTGCAGTCAAACAAT
GGGGAATGTGCACTGGTGGTGTTTGGGGCCGTTCCCAGTATGACTACTGGGGCCAGGGGA
CCCAGGTCACCGTCTCCTCAGGATCCCTTCCTGAAACTGGT

Peptide:
QVQLQESGGGLVQPGASLRLSCVSAFSLDHYSVAWFRQAPGKEREGVSCHSRSNKATDYAD
SVKGRFTISRDSAKRTVYLQMNNLKPEDTAVYYCAVKQWGMCTGGVWGRSQYDYWGQGT
QVTVSSGSLPETGGHHHHHH

References

1. *Strebhardt, K.; Ullrich, A. Paul Ehrlich's magic bullet concept: 100 years of progress. Nature Reviews. Cancer **2008**, 8 (6) 473.*
2. Allavena, P.; Sica, A.; Solinas, G.; Porta, C.; Mantovani, A. The inflammatory micro-environment in tumor progression: The role of tumor-associated macrophages *Crit. Rev. Oncol. Hematol.* **2008**, *66* (1), 1.
3. Forssell, J.; Oberg, A.; Henriksson, M. L.; Stenling, R.; Jung, A.; Palmqvist, R. HighMacrophage Infiltration along the Tumor Front Correlates with Improved Survival in Colon Cancer *Clin. Cancer Res.* **2007**, *13* (5), 1472.
4. Tran, N.P.; Hung, C.F.; Roden, R.; Wu, T.C. Control of HPV infection and related cancer through vaccination. *Recent Results in Cancer Research* **2014,** *193*, 149.
5. Brahmer, J.R.; Pardoll, D.R. Immune Checkpoint Inhibitors: Making Immunotherapy a Reality for the Treatment of Lung Cancer. *Cancer Immunol Res* **2013**, *1*, 85.
6. *Litman, G.W.; Rast, J.P.; Shamblott, M.J.; Haire, R.N.; Hulst, M.; Roess, W.; Litman, R.T.; Hinds-Frey, K.R.; Zilch, A.; Amemiya, C.T. Phylogenetic diversification of immunoglobulin genes and the antibody repertoire. Mol. Biol. Evol. **1993**, 10 (1), 60.*
7. Brahmer, J. R.; Tykodi, S. S.; Chow, L. Q. M.; Hwu, W.-J.; Topalian, S. L.; Hwu, P.; Drake, C. G.; Camacho, L. H.; Kauh, J.; Odunsi, K.; Pitot, H. C.; Hamid, O.; Bhatia, S.; Martins, R.; Eaton, K.; Chen, S.; Salay, T. M.; Alaparthy, S.; Grosso, J. F.; Korman, A. J.; Parker, S. M.; Agrawal, S.; Goldberg, S. M.; Pardoll, D. M.; Gupta, A.; Wigginton, J. M. Safety and Activity of Anti–PD-L1 Antibody in Patients with Advanced Cancer *N. Engl. J. Med.* **2012**, *366* (26), 2455.
8. Lipson, E. J.; Sharfman, W. H.; Drake, C. G.; Wollner, I.; Taube, J. M.; Anders, R. A.; Xu, H.; Yao, S.; Pons, A.; Chen, L.; Pardoll, D. M.; Brahmer, J. R.; Topalian, S. L. Durable Cancer Regression Off-treatment and Effective Reinduction Therapy with an Anti-PD-1 Antibody *Clin. Cancer Res. Off. J. Am. Assoc. Cancer Res.* **2013**, *19* (2), 462.
9. Hamblett, K.J.; Senter, P.D.; Chace, D.F.; Sun, M.M.C.; Lenox, J.; Cerveny, C.G.; Kissler, K.M. Bernhardt, S.X.; Kopcha, A.K.; Zabinski, R.F.; Meyer, D.L.; Francisco, J.A Effects of Drug Loading on the Antitumor Activity of a Monoclonal Antibody Drug Conjugate *Clin Cancer Res.* **2004** *10*, 7063.
10. Presta, L.G.; Chen, H. O'Connor, S.J.; Chisholm, V.; Meng, Y.G.; Rummen, L.; Winkler, M.; Ferrara, N. Humanization of an Anti-Vascular Endothelial Growth Factor Monoclonal Antibody for the Therapy of Solid Tumors and Other Disorders *Cancer Res.* **1997** *57*, 4593
11. Kobayashi, K.; Sasaki, T.; Takenaka, F.; Yakushiji, H.; Fujii, Y.; Kishi, Y.; Kita, s.; Shen, L.; Kumon, H.; Matsuura, E. A Novel PET Imaging Using ^{64}Cu-Labeled Monoclonal Antibody against Mesothelin Commonly Expressed on Cancer Cells *J Immunol Res.* **2015**, 268172.
12. Boellaard, R.; O'Doherty, M. J.; Weber, W. A.; Mottaghy, F. M.; Lonsdale, M. N.; Stroobants, S. G.; Oyen, W. J. G.; Kotzerke, J.; Hoekstra, O. S.; Pruim, J.; Marsden, P. K.; Tatsch, K.; Hoekstra, C. J.; Visser, E. P.; Arends, B.; Verzijlbergen, F. J.; Zijlstra, J. M.; Comans, E. F. I.; Lammertsma, A. A.; Paans, A. M.; Willemsen, A. T.; Beyer, T.; Bockisch, A.; Schaefer-Prokop, C.; Delbeke, D.; Baum, R. P.; Chiti, A.; Krause, B. J. *Eur. J. Nucl. Med. Mol. Imaging* **2010**, *37* (1), 181.

13. Tavare, R.; McCracken, M. N.; Zettlitz, K. A.; Knowles, S. M.; Salazar, F. B.; Olafsen, T.; Witte, O. N.; Wu, A. M. Engineered antibody fragments for immuno-PET imaging of endogenous CD8+ T cells *in vivo Proc. Natl. Acad. Sci.* **2014**, *111* (3), 1108.
14. Rashidian, M.; Keliher, E. J.; Bilate, A. M.; Duarte, J. N.; Wojtkiewicz, G. R.; Jacobsen, J. T.; Cragnolini, J.; Swee, L. K.; Victora, G. D.; Weissleder, R.; Ploegh, H. L. Noninvasive imaging of immune responses *Proc. Natl. Acad. Sci. U. S. A.* **2015**.
15. Rashidian, M.; Keliher, E. J.; Dougan, M.; Juras, P. K.; Cavallari, M.; Wojtkiewicz, G. R.; Jacobsen, J. T.; Edens, J. G.; Tas, J. M. J.; Victora, G.; Weissleder, R.; Ploegh, H. Use of ^{18}F-2-Fluorodeoxyglucose to Label Antibody Fragments for Immuno-Positron Emission Tomography of Pancreatic Cancer *ACS Cent. Sci.* **2015**, *1* (3), 142
16. Dijkers, E. C.; Oude Munnink, T. H.; Kosterink, J. G.; Brouwers, A. H.; Jager, P. L.; de Jong, J. R.; van Dongen, G. A.; Schröder, C. P.; Lub-de Hooge, M. N.; de Vries, E. G. Biodistribution of 89Zr-trastuzumab and PET imaging of HER2-positive lesions in patients with metastatic breast cancer. *Clin. Pharmacol. Ther.* **2010**, *87* (5), 586.
17. Elsässer-Beile, U.; Reischl, G.; Wiehr, S.; Bühler, P.; Wolf, P.; Alt, K.; Shively, J.; Judenhofer, M. S.; Machulla, H.-J.; Pichler, B. J. PET imaging of prostate cancer xenografts with a highly specific antibody against the postate specific membrane antigen. *J. Nucl. Med. Off. Publ. Soc. Nucl. Med.* **2009**, *50* (4), 606.
18. Vosjan, M. J. W. D.; Perk, L. R.; Visser, G. W. M.; Budde, M.; Jurek, P.; Kiefer, G. E.; van Dongen, G. A. M. S. Conjugation and radiolabeling of monoclonal antibodies with zirconium-89 for PET imaging using the bifunctional chelate p-isothiocyanatobenzyl-desferrioxamine. *Nat. Protoc.* **2010**, *5* (4), 739.
19. Holliger, P.; Prospero, T.; Winter, G."Diabodies": Small bivalent And bispecific antibody fragments *Proc .Natl. Acad. Sci. USA* **1993** *90*: 6444
20. Huston, J.S.; Levinson, D.; Mudgett-Hunter, M.; Tai, M.S.; Novotný, J.; Margolies, M.N.; Ridge R.J.; Bruccoleri, R.E.; Haber, E.; Crea, R. Protein engineering of antibody binding sites: recovery of specific activity in an anti-digoxin single-chain Fv analogue produced in Escherichia coli. *Proc. Natl. Acad. Sci. U S A.* **1988** *85*(16): 5879.
21. *Harmsen, M.M.; De Haard, H.J. Properties, production, and applications of camelid single-domain antibody fragments. Appl. Microbiol. Biotechnol.* ***2007*** *77 (1): 13.*
22. Rashidian, M.; Keliher, E. J.; Bilate, A. M.; Doarte, J.; Wojtkiewicz, G.; Jacobsen, J.; Victora, G.; Weissleder, R.; Ploegh, H. L. Noninvasive imaging of immune responses. *Proc. Natl. Acad. Sci. U.S.A.* **2015** *112*(19): 6146.
23. Smolarek, D.; Bertrand, O.; Czerwinski, M. Variable fragments of heavy chain antibodies (VHHs): a new magic bullet molecule of medicine? *Postępy Hig. Med. Dośw. Online* **2012**, *66*, 348.
24. Broisat, A.; Hernot, S.; Toczek, J.; De Vos, J.; Riou, L. M.; Martin, S.; Ahmadi, M.; Thielens, N.; Wernery, U.; Caveliers, V.; Muyldermans, S.; Lahoutte, T.; Fagret, D.; Ghezzi, C.; Devoogdt, N. Nanobodies targeting mouse/human VCAM1 for the nuclear imaging of atherosclerotic lesions. *Circ. Res.* **2012**, *110* (7), 927.
25. Chakravarty, R.; Goel, S.; Cai, W. Nanobody: The "Magic Bullet" for Molecular Imaging? *Theranostics* **2014**, *4* (4), 386.
26. De Meyer, T.; Muyldermans, S.; Depicker, A. Nanobody-based products as research and diagnostic tools. *Trends Biotechnol.* **2014**, *32* (5), 263.

27. Xavier, C.; Vaneycken, I.; D'huyvetter, M.; Heemskerk, J.; Keyaerts, M.; Vincke, C.; Devoogdt, N.; Muyldermans, S.; Lahoutte, T.; Caveliers, V. Synthesis, preclinical validation, dosimetry, and toxicity of 68Ga-NOTA-anti-HER2 Nanobodies for iPET imaging of HER2 receptor expression in cancer. *J. Nucl. Med. Off. Publ. Soc. Nucl. Med.* **2013**, *54* (5), 776.
28. Chatalic, K. L. S.; Veldhoven-Zweistra, J.; Bolkestein, M.; Hoeben, S.; Koning, G. A.; Boerman, O. C.; de Jong, M.; van Weerden, W. M. A novel 111In-labeled anti-PSMA nanobody for targeted SPECT/CT imaging of prostate cancer. *J. Nucl. Med. Off. Publ. Soc. Nucl. Med.* **2015**, *56* (7), 1094.
29. Ton-That, H.; Liu, G.; Mazmanian, S.K.; Faull, K.F.; Schneewind, O. Purification and characterization of sortase, the transpeptidase that cleaves surface proteins of *Staphylococcus aureus* at the LPXTG motif. *Proc. Natl. Acad. Sci.* **1999** *96*(22), 12424.
30. Merrifield, R.B. Solid Phase Peptide Synthesis. I. The Synthesis of a Tetrapeptide. *J. Am. Chem. Soc.* **1993** 85(14), 2149.
31. Albericio, F. Solid-Phase Synthesis: A Practical Guide (1 ed.). Boca Raton: *CRC Press.* **2000**, 848.
32. Schnolzer, M. A.; P.; Jones, A.; Alewood, D.; Kent, S.B.H. In Situ Neutralization in Boc-chemistry Solid Phase Peptide Synthesis. *Int. J. Peptide Res. Therap.* **2007** 13 (1-2), 31.
33. Nilsson, B.L.; Soellner, M.B.; Raines, R.T. Chemical Synthesis of Proteins. *Annu. Rev. Biophys. Biomol. Struct.* **2005** 34: 91.
34. Hruby, V.J.; Barstow, L.E.; Linharrt, T. New machine for automated solid phase peptide synthesis *Anal. Chem.*, **1972** 44 (2), 343.
35. Roovers, R. C.; Vosjan, M. J. W. D.; Laeremans, T.; el Khoulati, R.; de Bruin, R. C. G.; Ferguson, K. M.; Verkleij, A. J.; van Dongen, G. A. M. S.; van Bergen en Henegouwen, P. M. P. A biparatopic anti-EGFR nanobody efficiently inhibits solid tumour growth *Int. J. Cancer J. Int. Cancer* **2011**, 129 (8), 2013.
36. Mukherjee, J.; Tremblay, J. M.; Leysath, C. E.; Ofori, K.; Baldwin, K.; Feng, X.; Bedenice, D.; Webb, R. P.; Wright, P. M.; Smith, L. A.; Tzipori, S.; Shoemaker, C. B. A novel strategy for development of recombinant antitoxin therapeutics tested in a mouse botulism model. *PLoS ONE* **2012**, 7 (1), e29941.
37. De Genst, E.; Silence, K.; Decanniere, K.; Conrath, K.; Loris, R.; Kinne, J.; Muyldermans, S.; Wyns, L. Molecular basis for the preferential cleft recognition by dromedary heavy-chain antibodies. *Proc. Natl. Acad. Sci. U. S. A.* **2006**, *103* (12), 4586.
38. Younggyu Kim, Sam O. Ho, Natalie R. Gassman, You Korlann, Elizabeth V. Landorf, Frank R. Collart, and Shimon Weiss. Efficient Site-Specific Labeling of Proteins via Cysteines *Bioconjug Chem.* **2008** *19*(3), 786.
39. Blackman, M. L.; Royzen, M.; Fox, J. M. The Tetrazine Ligation: Fast Bioconjugation based on Inverse-electron-demand Diels-Alder Reactivity *J. Am. Chem. Soc.* **2008**, *130* (41), 13518.
40. David Sheehan and Siobhan O'Sullivan. Fast Protein Liquid Chromatography. *Protein purification protocols.* **2004** *244*, 253.
41. Baskin, J. M.; Prescher, J. A.; Laughlin, S. T.; Agard, N. J.; Chang, P. V.; Miller, I. A.; Lo, A.; Codelli, J. A.; Bertozzi, C. R. Copper-free click chemistry for dynamic in vivo imaging. *Proc. Natl. Acad. Sci.* **2007**, *104* (43), 16793.
42. Denk, W.; Strickler, J.H.; Webb, W.W. Two-photon laser scanning fluorescence microscopy. *Science* **1990**, *248*(4951), 73.

43. Chen, I.; Dorr, B. M.; Liu, D. R. A general strategy for the evolution of bond-forming enzymes using yeast display. *Proc. Natl. Acad. Sci. U. S. A.* **2011** *108*, 11399
44. Theile, C. S.; Witte, M. D.; Blom, A. E. M.; Kundrat, L.; Ploegh, H. L.; Guimaraes, C. P. Site-specific N-terminal labeling of proteins using sortase-mediated reactions. *Nat. Protoc.* **2013** *8*, 1800
45. Witte, M. D.; Cragnolini, J. J., Dougan, S. K.; Yoder, N. C.; Popp, M. W.; Ploegh, H. L. Preparation of unnatural N-to-N and C-to-C protein fusions. *Proc. Natl. Acad. Sci* **2012** *109*, 11993.

Acknowledgements

Thanks to Hidde Ploegh for giving me the opportunity to work in his lab. Thanks to Mohammad Rashidian for supervision and teaching about biology and chemistry. Thanks to all the Ploegh lab members for their help and guidance. Finally thanks to Maarten Linskens for supervision on behalf of the University of Groningen.